2007-01-2365

# Transient Response of Hydraulic Engine Mount to a Realistic Excitation: Improved Non-Linear Models and Validation

**Song He and Rajendra Singh**
Acoustics and Dynamics Laboratory
The Ohio State University



## ABSTRACT

Competing linear, quasi-linear and non-linear hydraulic mount formulations of fixed and free decoupler types are comparatively evaluated for transient responses. First, features of the realistic excitation conditions are addressed. For instance, the mean load itself may vary with time, and several sinusoidal or transient excitations may be simultaneously present. Second, a multi-staged top chamber compliance model is proposed to capture asymmetric transient responses given step-up (-down) excitations. Third, implicit excitations introduced by the decoupler switching mechanism are identified at the odd harmonics of the explicit excitation frequency. Fourth, discontinuous model of bottom chamber compliance is proposed depending on the operating point(s) and/or dynamic loading. Some of the discrepancies observed between prior models and measurements can be explained using new models.

## INTRODUCTION

Hydraulic engine mount is designed to be highly non-linear as its parameters, such as stiffness and damping parameters, significantly vary with the amplitude ($X$) and frequency ($f$) of sinusoidal excitation [1-15]. Over the past two decades, extensive experimental and analytical studies have been conducted on the non-linear characterization under steady state condition [1-8], but their non-linear behaviors under transient or arbitrary loading excitations (say with multiple frequency components) are not well understood. To better illustrate the full extent of the underlying research issues, consider the fluid system of Fig. 1, where control volumes are used to describe a free decoupler type mount [2,9-10]. System parameters include the fluid compliances $C_1$ and $C_2$ of the top (#1) and bottom (#2) chambers, stiffness $k_r$ and viscous damping $b_r$ of the elastomeric rubber element (#$r$), fluid resistance $R_i$ and inertance $I_i$ of the inertia track (#$i$), inertance $I_d$ and resistance $R_d$ of the decoupler (#$d$). A composite displacement $x^t(t)$ is applied as an excitation under a preload $F_m$. In general, one should expect the following elements to exhibit non-linear behaviors: (i) non-linear compliances $C_1(p_1)$ and $C_2(x_m)$ due to elastomeric walls where $p_1(t)$ is the dynamic pressures in the top chamber [9-10] and $x_m(t)$ is the (time-varying) mean displacement; (ii) vacuum formation in the top chamber during the expansion process [2, 10]; (iii) non-linear resistances $R_i(q_i)$ and $R_d(q_d)$ where $q_i(t)$ and $q_d(t)$ are the volumetric flow rates through the inertia track and decoupler, respectively [9-10]; and (iv) the switching mechanism of the decoupler [9-10]. In this paper, we intend to illustrate the roles played by the non-linear chamber compliances and the decoupler switching mechanism, especially under transient and multi-frequency loading conditions.

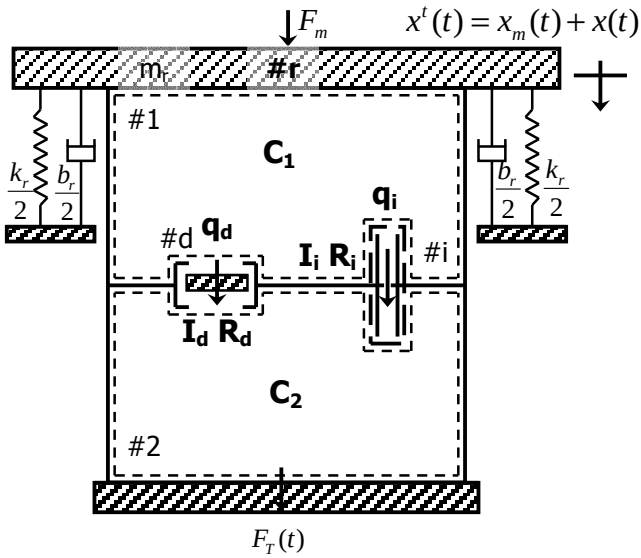


Fig. 1 Lumped fluid model of hydraulic mount with inertia track and decoupler.

## PRIOR TESTS AND NON-LINEAR MODELS

Kim and Singh [1-2] initiated the non-linear analysis of hydraulic mounts by measuring non-linear $C_1$, $C_2$ and $R_i$ of a fixed decoupler mount via bench experiments [1]. They successfully formulated a non-linear model that included a preliminary formulation of the decoupler switching mechanism, under harmonic excitations [2]. Colgate et al. [3] tested several mounts under concurrent

sinusoidal excitations and then proposed two separate linear models for large and small amplitudes. Royston and Singh [4] employed Kim and Singh's model [2] as a localized non-linearity and examined its effect on the vibratory power transmission. Jeong and Singh [5] suggested a non-linear time domain model based on a quasi-linear model with frequency- and amplitude-dependent parameters. Empirical coefficients were obtained by observing the effects of resonant frequencies and viscous damping coefficients given measured mount stiffness data. Geisberger et al. [6] tested the top and bottom fluid chambers, inertia track and decoupler. They proposed a non-linear model that, in particular, utilizes a smoothening function to describe the switching and leakage effects through the decoupler. Jazar and Golnaraghi [7] proposed a simple non-linear mathematical model to characterize the decoupler resistance in terms of the Duffing's equation (continuous non-linearity). Foumani et al. [8] conducted a sensitivity analysis and concluded that $C_1$ and $I_i$ are the most influential parameters in the dynamic stiffness model over the lower frequency range. Tiwari et al. [9] refined the bench experiments [1] and further quantified $C_1$ and $C_2$ under several $F_m$. Also, they investigated the vacuum formation that was first mentioned by Kim and Singh [1-2]. Adiguna et al. [10] examined the mount behavior to idealized transient excitations and successfully predicted the transient responses based on non-linear formulations with empirically obtained parameters or functions. Recently, we proposed an efficient procedure to estimate the frequency- and amplitude-sensitive parameters based on measured steady state dynamic stiffness data [11]. This work has led to the construction of quasi-linear models. Such models are capable of partially predicting the transient response. Nonetheless, some of the discrepancies between predictions and measurements could not be explained by the quasi-linear model.

## PROBLEM FORMULATION

Though some non-linear models have been proposed and validated to some extent, one key question still remains: Do we really know all of the non-linearities in such mounts? Also, which non-linearities would be excited under realistic excitation conditions, especially when $F_m$ itself may also vary with time, and when several sinusoidal or transient excitations may be simultaneously present? Further, we need to comparatively evaluate the competing linear, quasi-linear and non-linear formulations. Accordingly, the following objectives have been formulated: First, classify the displacement excitation conditions and illustrate some features of a realistic (measured) displacement profile that will be applied to the models as an excitation. Second, examine the role of decoupler as it could generate an implicit displacement excitation to the system. Third, propose the discontinuous model $C_2$ and examine the associated non-linear phenomena. Finally, validate the new non-linear formulations by comparing $p_1(t)$ and transmitted force $F_T(t)$ in both time and frequency domains given realistic excitations.

In this paper, we will summarize only those equations that are necessary for further development of the non-linear model of Fig. 1. Considering only the time-varying components, the "virtual" driving point force $F(t)$ could be defined as follows where $x(t)$ is the piston displacement, $m_r$ is the mass of rubber element and $A_r$ is the effective piston area.

$$F(t) = m_r \ddot{x}(t) + b_r \dot{x}(t) + k_r x(t) + A_r p_1(t) \tag{1}$$

Continuity equations for the top and bottom chambers of Fig. 1 yield:

$$A_r \dot{x}(t) - q_i(t) - q_d(t) = C_1(p_1)\dot{p}_1(t), \tag{2}$$

$$q_i(t) + q_d(t) = C_2(x_m)\dot{p}_2(t). \tag{3}$$

Momentum equations for the decoupler and inertia track yield the following:

$$p_1(t) - p_2(t) = I_d \dot{q}_d(t) + R_d(q_d) q_d(t), \tag{4}$$

$$p_1(t) - p_2(t) = I_i \dot{q}_i(t) + R_i(q_i) q_i(t). \tag{5}$$

Note that Eq. (4) dictates the "decoupled" state when the decoupler gap is open, and Eq. (5) is dominant over the "coupled" state with the decoupler gap closes. The dynamic force transmitted to the rigid base $F_T^t(t)$ is often viewed as a measure of mount performance in non-resonant tests [1]. Its dynamic component $F_T(t)$ is derived and related to $F(t)$ as follows:

$$F_T(t) = k_r x(t) + b_r \dot{x}(t) + A_r p_1(t) = F(t) - m_r \ddot{x}(t). \tag{6}$$

## DISPLACEMENT EXCITED NON-LINEARITIES

Displacement excitation sources are clarified as: (a) explicit composite excitation $x^t(t) = x_m(t) + x(t)$ that is externally applied; and (b) implicit decoupler displacement $x_d(t)$. The mean component $x_m(t)$ includes the time-varying part $\Delta x(t)$ that could be of the same order of magnitude as the time-averaged $x^t(t)$. The dynamic component $x(t)$ corresponds to fluctuation $\Delta x(t)$ that is much smaller than $x_m(t)$. Using these groupings, we now examine the excitations of Fig. 2 and the associated non-linearities.

First, the sinusoidal excitation of Fig. 2(a) is commonly applied in dynamic stiffness measurement [1-8], where the constant $x_m$ (corresponding to a specific $F_m$) is usually neglected in the analysis, thus leaving only the sinusoidal component $x(t) = X \cdot \sin(2\pi f t + \phi)$. In steady state elastomer tests, the dynamic stiffness $K(f,X)$ is evaluated only at the frequency of excitation $f$ and super-harmonics are ignored [1-8]. A quasi-linear model could also be estimated from the $K(f,X)$ data [11].

Second, simple transient tests conducted under a constant $F_m$ or $x_m$, such as the triangular pulse excitation of Fig. 2(b) [9]. Transient responses to the special case of $x^t(t) = x_m(t) + x(t)$ have been partially predicted by the

quasi-linear model [11]. This implies that for an idealized transient excitation when applied at a certain loading condition specified by a constant $x_m$ (or $F_m$), the mount could behave as a linearized system and its effective parameters could be estimated by using the quasi-linear model [11]. We may employ the Fourier series to expand periodic $x(t)$ as $x(t) = \Sigma X_i \cdot \sin(2\pi f_i t + \phi_i)$, where $X_i$ is the Fourier amplitude.

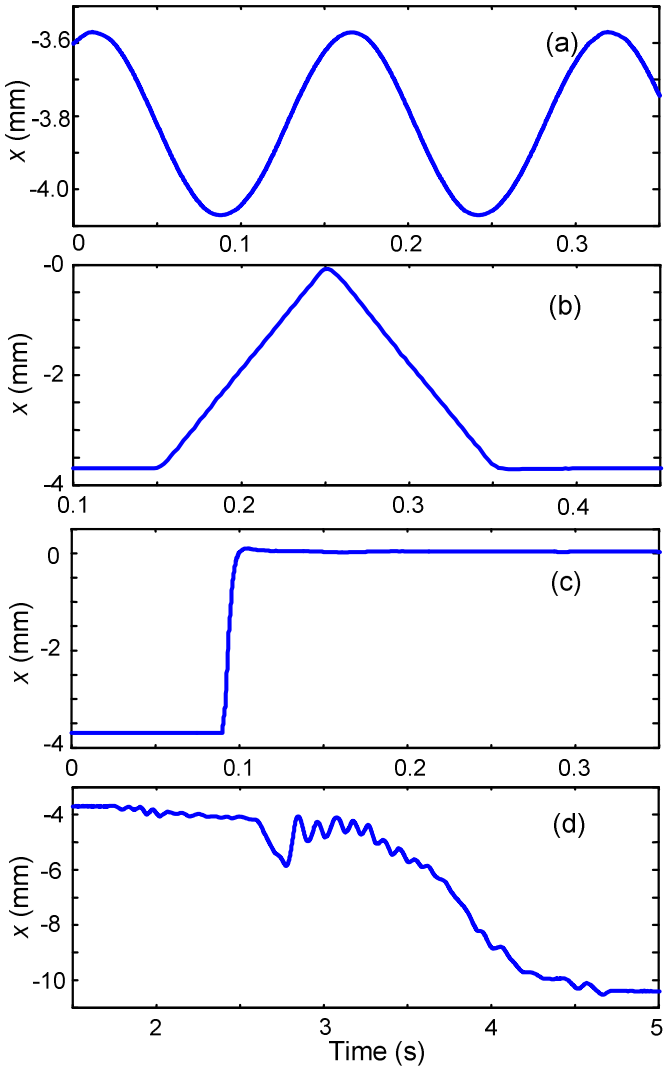


Fig. 2 Measured explicit displacement excitations: (a) sinusoidal excitation $x(t) = X\cdot\sin(2\pi ft+\phi)$; (b) simple triangular pulse excitation $x^t(t) = x_m + x(t)$; (c) step-up excitation with a non-ideal rise; and (d) a realistic excitation from the measurements in a vehicle.

Third, transient excitations are considered with a rapid change in the mean loading condition such as the step-up excitation in Fig. 2(c). Adiguna et al. [10] had briefly reported responses to such step-up (-down) excitations. Significant asymmetries were observed in the measured peak values of $F_T(t)$ and $p_1(t)$ for the step-up and step-down responses, suggesting that a different non-linear stage has been introduced. Denoting $x_{m,1}$ and $x_{m,2}$ as the operating conditions before and after the switching event, the step-up (-down) excitation is formulated as follows,

where $\Delta t$ represents the short time span during which the step function rises or drops (ideally $\Delta t \rightarrow 0$) due to the limitation of test facility:

$$x^t(t) = \begin{cases} x_{m,1} & 0 \le t < t_1 \\ x_{step}(\Delta t) & t_1 \le t < t_1 + \Delta t \\ x_{m,2} & t_1 + \Delta t < t \end{cases} \quad (7)$$

By using $p_1(t)$ as an indicator of the operating condition, a multi-staged $C_1(p_1)$ model could be developed to capture the asymmetric non-linearity:

$$C_1(p_1) = \begin{cases} C_{10} - a_V p_1^{n_V}(t) & p_1(t) < 0 \\ C_{10} & 0 \le p_1(t) \le p_a \\ C_{10} - a_S \left[p_1(t) - p_a\right]^{n_S} & p_a < p_1(t) \end{cases} . \quad (8)$$

Here, $C_{10}$ is the (constant) nominal compliance measured in the linear region. Empirical coefficients $a_V$ and $a_S$, polynomial order indices $n_V$ and $n_S$ could be estimated from measurements.

Fourth, the most complicated, yet realistic, excitations are considered, which may include the following terms: time-varying (piece-wise linear) $x_m(t)$ and dynamic $x(t)$ with multiple and non-commensurate sinusoids at $f_i$: $x^t(t) = x_{m,j-1} + \Gamma_j\left(t - t_{j-1}\right) + \sum_{i=1}^{n} X_i \sin(2\pi f_i t + \phi_i)$ . A constant slope $\Gamma_j = \left(x_{m,j} - x_{m,j-1}\right)/\left(t_j - t_{j-1}\right)$ is assumed within the $j^{th}$ segment, and a critical slope $\Gamma_c > \Gamma_j$ could be empirically chosen to distinguish $\Gamma_j$ from the rapid switching case of Eq. (7). The fluctuating $x(t)$ could be simplified by considering only the dominant sinusoidal excitation(s), say via the Fast Fourier Transform (FFT). The $x^t(t)$ of Fig. 2(d) was measured at the mount location in a front wheel drive vehicle during a typical gear shift event. This transient record contains approximately 3 seconds of data. Several oscillatory displacements (from 5 to 15 Hz) are superimposed on $x_m(t)$ that increases from -4 to -10.5 mm, corresponding to a shift in $F_m$ from -1200 to -4000 N. A piecewise non-linear $C_2(x_m)$ model is proposed here to fully capture the stiffening effect which gives rise to a significant increase in the mean chamber pressure as observed in measurements. Such details will be given later.

$$C_2(t) = C_{2,j-1} + \frac{C_{2,j} - C_{2,j-1}}{t_j - t_{j-1}}\left(t - t_{j-1}\right). \quad (9)$$

## MULTI-STAGED NON-LINEAR $C_1(P_1)$ MODEL

Compared with $C_2$, which dictates the mean chamber pressure, the $C_1(p_1)$ non-linearity plays a pivot role in transient mount behaviors. Consider the step-up (or step-down) excitation of Fig. 2(c) with a rapid change in the mean load, the multi-staged $C_1(p_1)$ model of Eq. (8) could be derived by analyzing the asymmetric step responses in terms of $F_T(t)$ and $p_1(t)$ measurements.

Experiments were conducted using a take-apart mount D with removable decoupler structure and its parameters are given in Table 1. Here, $C_{10}$ and $C_{20}$ are the linearized nominal values [9-10]; $m_d$ and $b_d$ are the mass and damping of the decoupler; $L_i$ and $L_g$ are the lengths of the inertia track and decoupler gap, respectively. Measurements of the fixed decoupler mount D are compared with predictions using quasi-linear models as shown in Figs. 3-6. Observe that the quasi-linear model fails to predict both the overshoot and the decaying transient due to significant $C_1$ non-linearity.

Table 1 Parameters of the example case (hydraulic mount D)

| | | | |
|---|---|---|---|
| $k_r$ | $320\times10^{3}$ N/m | $A_r$ | $3.31\times10^{-3}$ m$^2$ |
| $b_r$ | $0.5\times10^{3}$ N-s/m | $A_d$ | $1.96\times10^{-3}$ m$^2$ |
| $C_{10}$ | $2.5\times10^{-11}$ m$^5$/N | $R_i$ | $3.45\times10^{7}$ kg/s-m$^4$ |
| $C_{20}$ | $2.4\times10^{-9}$ m$^5$/N | $L_i$ | 0.236 m |
| $I_i$ | $2.81\times10^{6}$ kg/m$^4$ | $b_d$ | 100 N-s/m |
| $m_d$ | $6\times10^{-3}$ kg | $L_g$ | $1.1\times10^{-3}$ m |

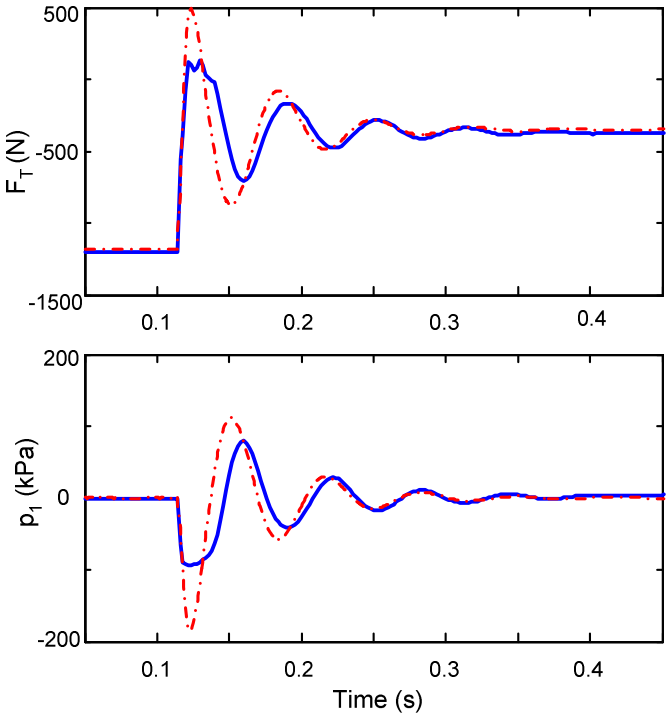


Fig. 3 Estimation of the effective $C_{1e}$ from step-up ($x_m$ from -3.7 to -1.32 mm) response by curve-fitting the decaying transients. Key: ——, measurement; - - -, simulation with estimated $C_{1e}$.

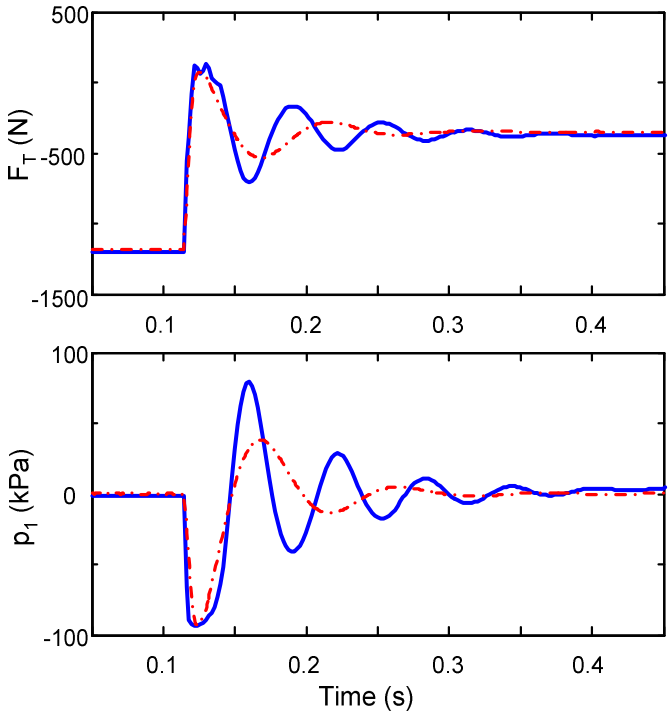


Fig. 4 Estimation of the effective $C_{1e}$ from step-up ($x_m$ from -3.7 to -1.32 mm) response by curve-fitting the overshoot. Key: ——, measurement; - - -, simulation with estimated $C_{1e}$.

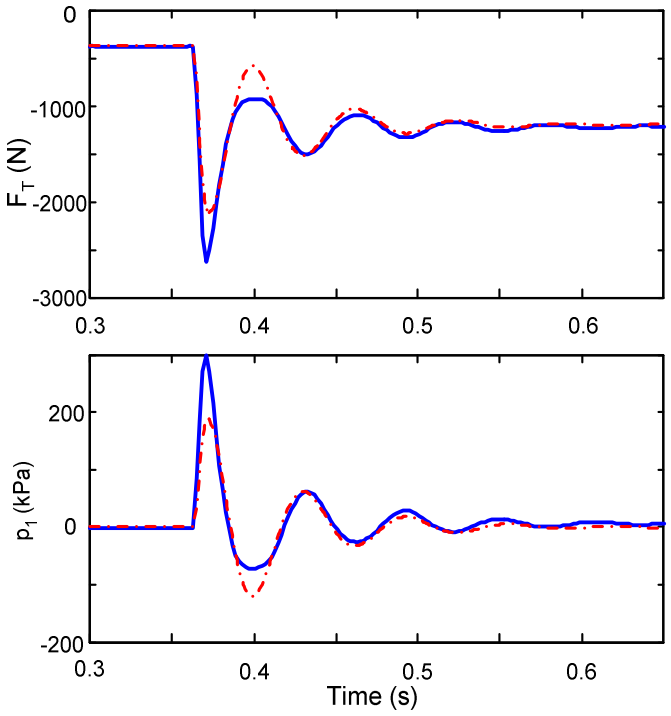


Fig. 5 Estimation of the effective $C_{1e}$ from step-down ($x_m$ from -1.32 to -3.7 mm) response by curve-fitting the decaying transients. Key: ——, measurement; - - -, simulation with estimated $C_{1e}$.

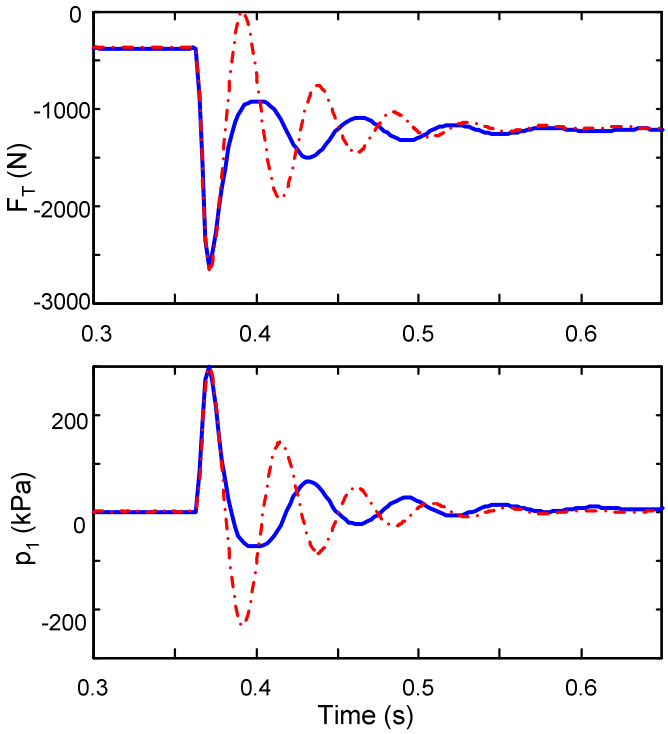


Fig. 6 Estimation of the effective $C_{1e}$ from step-down ($x_m$ from -1.32 to -3.7 mm) response by curve-fitting the overshoot. Key: ——, measurement; – · – ·, simulation with estimated $C_{1e}$.

As a first estimate, effective $C_{1e}$ values are approximated using the quasi-linear model [11] by best curve-fitting either the overshoot or decaying transient given various step excitations in Figs. 3-6. The curve-fitting results, as listed in Table 2(a), are compared with linearized $C_1$ values measured at several $F_m$ [9], as listed in Table 2(b). Comparison between Table 2(a) and 2(b) shows that $C_{1e}$ corresponding to the step-up overshoot (from -3.7 to 0 mm) is consistent with the statically measured $C_1$ under no preload; $C_{1e}$ estimated from the step-down overshoot (from 0 to -3.7 mm) coincides with $C_1$ measured under $F_m$ = -1200 N (or $x_m$ = -3.7 mm).

Table 2 Top chamber compliance $C_1$
(a) Effective $C_{1e}$ estimated from step-up or step-down responses.

| Excitation \ Estimated | From overshoot | From decay |
|---|---|---|
| | $C_{1e}$ ($m^5$/N) | $C_{1e}$ ($m^5$/N) |
| Step-up (-3.7 to 0 mm) | $7.63\times10^{-11}$ | $2.99\times10^{-11}$ |
| Step-up (-3.7 to -1.32 mm) | $5.28\times10^{-11}$ | $2.45\times10^{-11}$ |
| Step-down (0 to -3.7 mm) | $1.09\times10^{-11}$ | $2.39\times10^{-11}$ |
| Step-down (-1.32 to -3.7 mm) | $1.26\times10^{-11}$ | $2.17\times10^{-11}$ |

(b) Measured $C_1$ values from static tests [9-10]

| Condition | $F_m$ (N) | $C_1$ ($m^5$/N) |
|---|---|---|
| $p_1 > p_a$ | 0 | $7.29\times10^{-11}$ |
| | −800 | $1.05\times10^{-11}$ |
| | −1200 | $1.09\times10^{-11}$ |
| | −1200 | $2.5\times10^{-11}$ ($C_{10}$) |
| $p_1 < p_a$ | $C_1 = -7\times10^{-45}p_1^{7} + 2.5\times10^{-11}$ ($p_1$ in Pa) | |

It is implied that the overshoot transients are dictated by the operating conditions after the step takes place. On the other hand, $C_{1e}$ values estimated from the decay transients are consistent for all step responses. Also, note that these $C_{1e}$ (ranging from $2.17\times10^{-11}$ to $2.99\times10^{-11}$ $m^5$/N) match well with the nominal $C_{10}$ value ($2.5\times10^{-11}$ $m^5$/N), which is a linearized value based on several operational conditions [10]. The fact that $C_{10}$ lies between the effective $C_{1e}$ values estimated from step-up and step-down overshoots implies that (i) a dynamic softening effect exists during the unloading process. This could be explained by the vacuum phenomenon due to a release of the dissolved gas under reduced pressure, as suggested by Kim and Singh [1] and Adiguna et al. [10]. (ii) A dynamic stiffening effect takes control during the loading process. (iii) A linear region exists between the softening and hardening regions, in which a linearized (quasi-linear) model should be sufficient to predict transient responses. By using $p_1(t)$ as an indicator of the operating condition, the multi-staged $C_1(p_1)$ non-linearity is mathematically formulation by Eq. (8). For mount D, the empirical coefficients of Eq. (8) are estimated as: $a_V = 7\times10^{-45}$, $a_S = 1.55\times10^{-33}$, $n_V = 7$ and $n_S = 4$. Here, the linearized $C_{10} = 2.5\times10^{-11}$ $m^5$/N dictates the decaying response, and $p_a$ = 101 kPa is the limiting (atmospheric) pressure beyond which significant stiffening effect will occur. A detailed comparative study of the non-linear step-up (or step-down) transient responses will be reported in another paper [16].

## IMPLICIT DISPLACEMENT EXCITATION FROM DECOUPLER

The decoupler displacement $x_d(t)$ is dynamically coupled with instantaneous pressure difference $\Delta p(t)$, excitation amplitude $X$, excitation frequency $f$ and decoupler gap length $L_g$. In order to examine the decoupler dynamics, the take-apart mount D of Table 1 was tested both with and without (i.e. fixed decoupler type) the decoupler under the excitations of Figs. 2(a) and 2(d). Predicted $x_d(t)$ of the free decoupler mount D given sinusoidal excitations are shown in Figs. 7(a-c), and Fig. 7(d) shows the $x_d(t)$ given realistic profile excitation. Observe that the period of $x_d(t)$ coincides with the excitation period $T = 1/f$, but its shape derivates from the sinusoidal waveform. Consequently, $x_d(t)$ is categorized as an implicit displacement excitation.

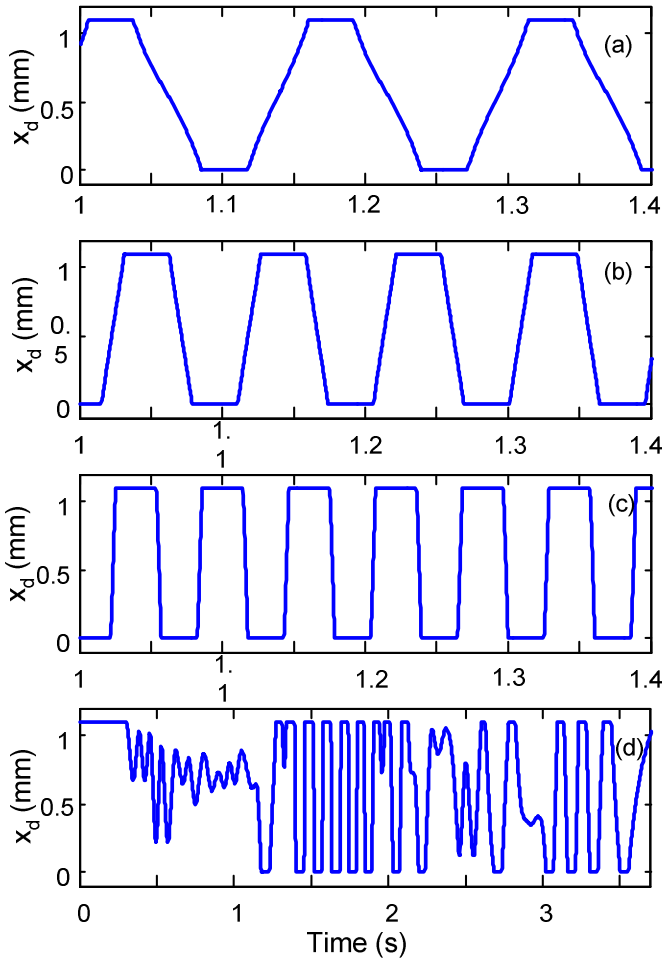


Fig. 7 Simulated decoupler displacements $x_d(t)$ given explicit displacement excitations: (a) sinusoidal $x(t)$ with $f$ = 6.5 Hz, $X$ = 0.5 mm; (b) sinusoidal $x(t)$ with $f$ = 10.5 Hz, $X$ = 0.5 mm; (c) sinusoidal $x(t)$ with $f$ = 16.5 Hz, $X$ = 0.5 mm; and (d) realistic excitation $x^t(t)$ of Fig. 2(d).

It is shown in Fig. 8 that simulated steady state time histories match well with measurements as excited by a sinusoidal excitation with $f$ = 12.5 Hz and $X$ = 0.5 mm (p-p), under $F_m$ = 1200 N (or $x_m$ = 3.7 mm). Observe that the decoupler switching mechanism distorts the sinusoidal-like $p_1(t)$ and $F_T(t)$ waveforms (of a fixed decoupler mount) by introducing flattened regions whenever the decoupler gap opens.

Further, the Fast Fourier Transform (FFT) routine is used to convert time histories into frequency domain and spectra of Fourier series amplitudes are depicted in Fig. 9. Compared with $X(f)$, the $X_d(f)$ spectrum shows discrete peaks not only at the external excitation frequency (12.5 Hz), but also at the 3rd harmonic (37.5 Hz) and higher odd harmonics. Fig. 10 shows $P_1(f)$ and $F_T(f)$ spectra for fixed and free decoupler mounts (D) converted from the time histories of Fig. 8. Both measurements and predictions show a significant increase only at the 3rd and higher odd harmonics for the free decoupler mount, which implies that $x_d(t)$ introduces an implicit excitation at the odd harmonics of external excitation frequency.

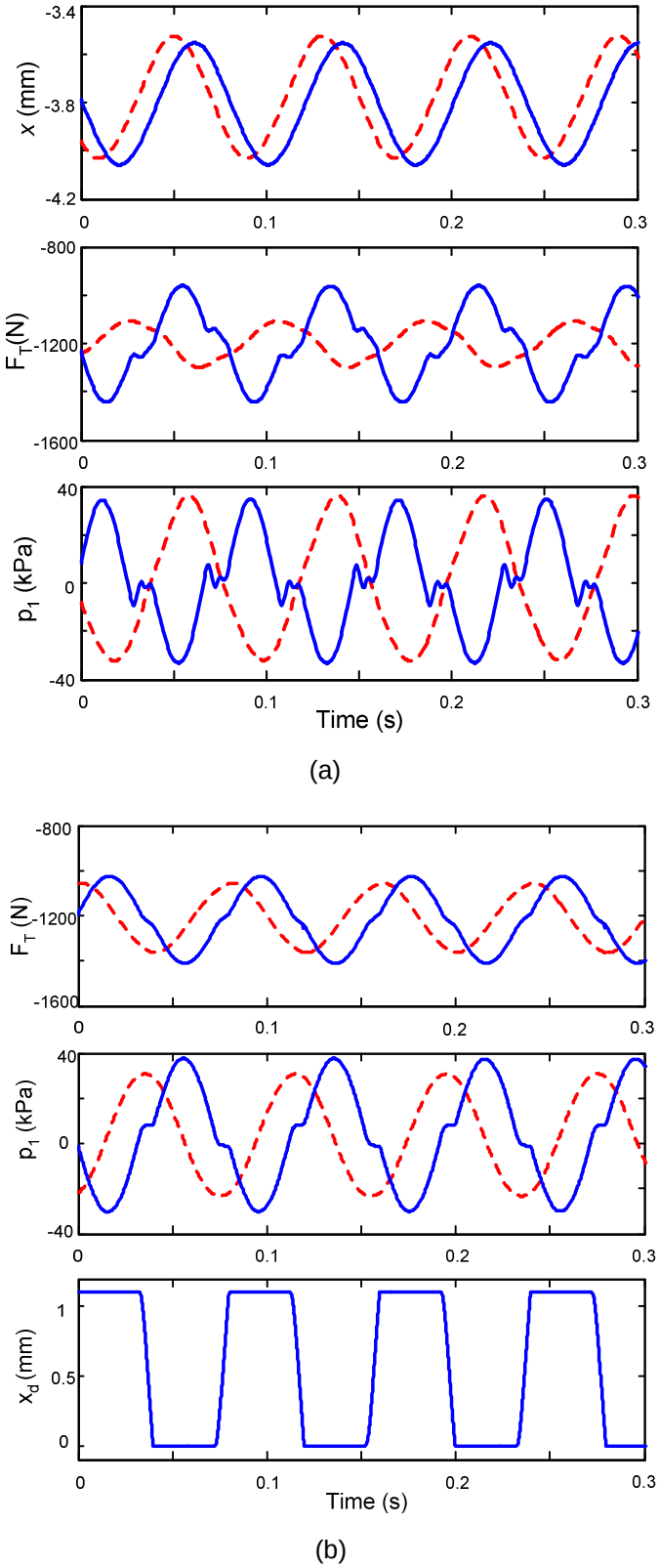


Fig. 8 Dynamic responses of free and fixed decoupler mount D given sinusoidal excitation with $f$ = 12.5 Hz and $X$ = 0.5 mm (p-p), under $F_m$ = 1200 N (or $x_m$ = 3.7 mm): (a) measurement; (b) simulation. Key: ——, free decoupler mount; – – –, fixed decoupler mount.

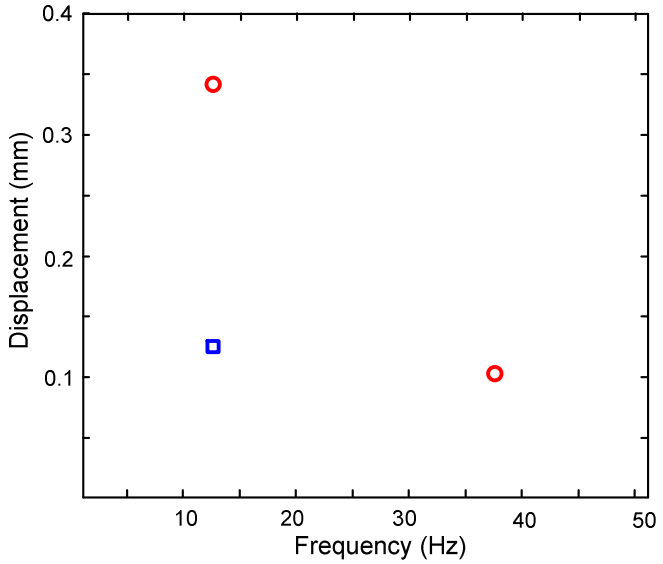


Fig. 9 Fourier amplitudes of displacements in Fig. 8. Key: ◘, explicit displacement excitation $X(f)$; O, implicit displacement excitation $X_d(f)$.

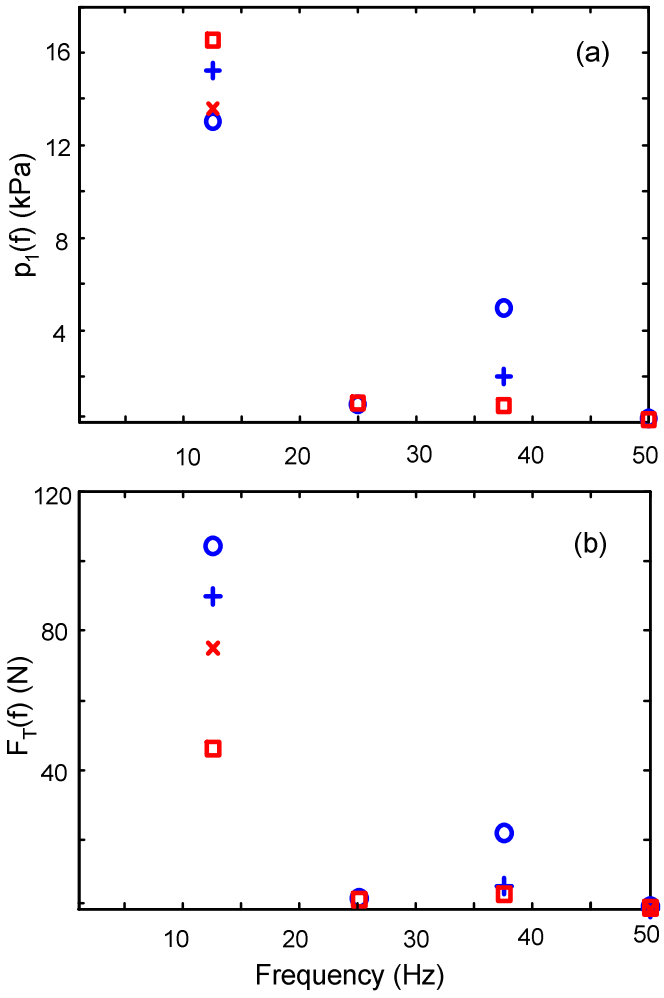


Fig. 10 Fourier amplitudes of $p_1(t)$ and $F_T(t)$ in Fig. 8: (a) top chamber pressure $p_1(f)$; (b) transmitted force $F_T(f)$. Key: O, measurement of free decoupler mount; +, measurement of fixed decoupler mount; ◘, simulation of free decoupler mount; ×, simulation of fixed decoupler mount.

Similar to the sinusoidal excitation responses, the implicit $x_d(t)$ excitation also plays a key factor given the realistic profile excitation of Fig. 2(d). Predicted transient responses are given in Fig. 7(d) and compared with measurements as shown later in Fig. 12. An in-depth analytical study will be reported in a future paper [16].

## DUAL-STAGED $C_2(X_M)$ NON-LINEARITY

Constructed using convoluted thin rubber membranes [9], the bottom chamber is intentionally designed to yield a large $C_2$ to accommodate fluid displaced from the top chamber. Due to the difficulty of analytically calculating $C_2$, most researchers [1-5,8-10] assumed a linearized (constant) $C_2$ value, which could be curve-fitted from measurements at a certain operating point. For instance, a nominal value $C_{20}$ of $2.4\times10^{-9}$ $m^5/N$ was measured for mount D and it seems to work well for triangular excitations under a preload $F_m$ of 1200 N. Note that $F_m$ (or $x_m$) plays a pivot role on the chamber compliances [2,9-10]: First, $F_m$ determines the operating point about which the non-linear compliances are estimated; second, $F_m$ dictates the mean fluid pressure (under the static equilibrium). This is because typically $C_2 >> C_1$ by two orders of magnitude [2,9-10], so that the global compliance of the fluid system is dictated by $C_2$. For example, the mean pressure measured by Adiguna et al. [10] is virtually equal to the atmospheric pressure when $F_m < 800$ N.

However, under real-life operational conditions with time-varying $F_m$ (or $x_m$), when more displaced fluid (from the top chamber) is accommodated, the bottom chamber membrane expands and gradually tends to lose its essential property as a very compliant accumulator. Hence, the reduced $C_2$ under higher $F_m$ (or $x_m$) leads to an increase in the mean chamber pressure, which could be observed from measurements in Figs. 11 and 12. A non-linear $C_2(x_m)$ model is proposed and demonstrated by considering the realistic $x^t(t) = x_m(t) + x(t)$ of Fig. 2(d). A piecewise linear $x_m(t)$ is derived as follows:

$$x_m(t) = x_{m,j-1} + \left(x_{m,j} - x_{m,j-1}\right)\frac{t - t_{j-1}}{t_j - t_{j-1}}, \qquad (10a)$$

By using $x_m(t)$ as an indicator to capture the gradual transition in the operation conditions, a piecewise $C_2(x_m)$ model could be found as:

$$C_2(x_m) = C_{2,j-1} + \left(C_{2,j} - C_{2,j-1}\right)\frac{x_m(t) - x_{m,j-1}}{x_{m,j} - x_{m,j-1}}, \qquad (10b)$$

By combining Eqs. (10a) and (10b), a simplified time-varying $C_2(t)$ could be derived as already given in Eq. (9). Despite the seemingly piecewise linear formulation, incorporation of $C_2(x_m)$ or $C_2(t)$ leads to non-linear fluid system model. A comparative study is conducted using (i) the quasi-linear model [11]; (ii) non-linear fluid model with a constant $C_{20}$; (iii) the non-linear $C_2(x_m)$ model. Fig. 11 confirms that the mean pressure built-up effect could only be captured by the $C_2(x_m)$ model while the quasi-

linear model is capable of predicting the transient dynamic responses.

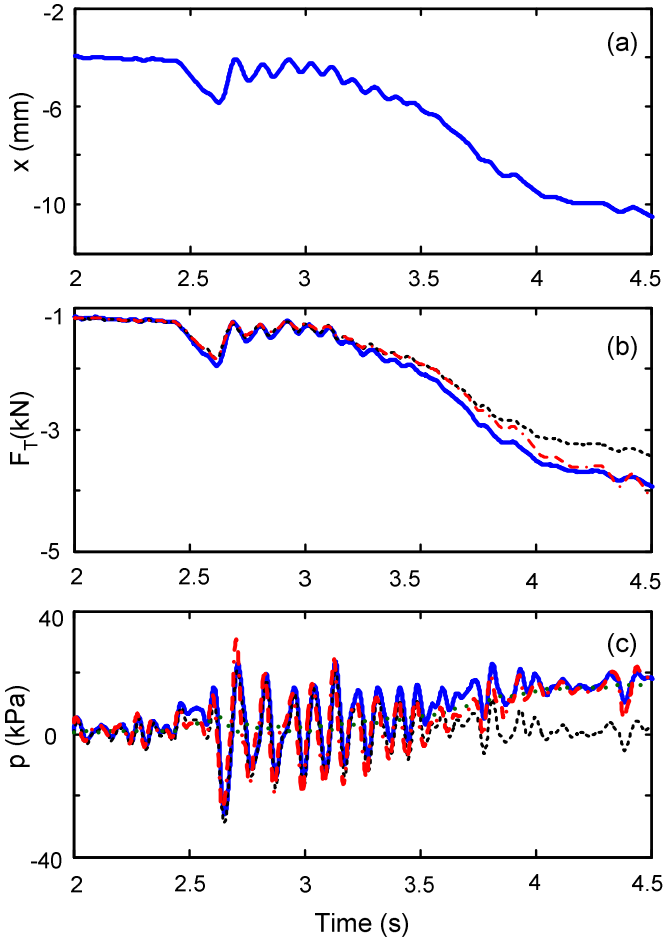


Fig. 11 Responses to a realistic profile excitation for a fixed decoupler mount D: (a) displacement excitation $x(t)$; (b) transmitted force $F_T(t)$; and (c) chamber pressures. Key: -·-·-, measurement; ----- quasi-linear model prediction; ——, non-linear $C_2(x_m)$ model prediction; · · · ·, non-linear $C_2(x_m)$ model prediction of $p_2(t)$ with $C_{2e} = C_{20}/1.8$.

Next, the realistic profile is applied to excite the free decoupler mount D. Measurements are compared with the non-linear models with nominal $C_{20}$ and $C_{2e}(x_m)$ formulations, as illustrated in Fig. 12. The quasi-linear model is not intentionally used since it would not adequately describe the decoupler non-linearity. Observe that the stiffening effect of $C_2$ becomes increasingly dominant under higher $F_m$ (or $x_m$). Finally, predictions match with measurements when $C_2(x_m > 8 \text{ mm}) = C_{20}/5$.

## CONCLUSION

Chief contribution of this paper is the identification and validation of new non-linearities as excited by realistic excitations with time-varying mean and several oscillation components. A generic category is proposed to understand mount non-linearities in terms of explicit displacement excitations and implicit excitation, which is introduced by the decoupler at the odd harmonics of the (explicit) fundamental frequency. A multi-staged $C_1(p_1)$ non-linear model is proposal to capture the asymmetric transient response given step-up (-down) excitations. A non-linear $C_2(x_m)$ model is developed depending on the operating point(s) and/or dynamic loading. New non-linear phenomena are explained by the multi-staged (and time-varying) descriptions of $C_2$. Competing linear, quasi-linear and non-linear formulations are comparatively evaluated. Finally, the new or refined non-linear formulations are validated by comparing predictions with measurements. Results match well in both time and frequency domains. More mathematical details and results can be found in upcoming article [16].

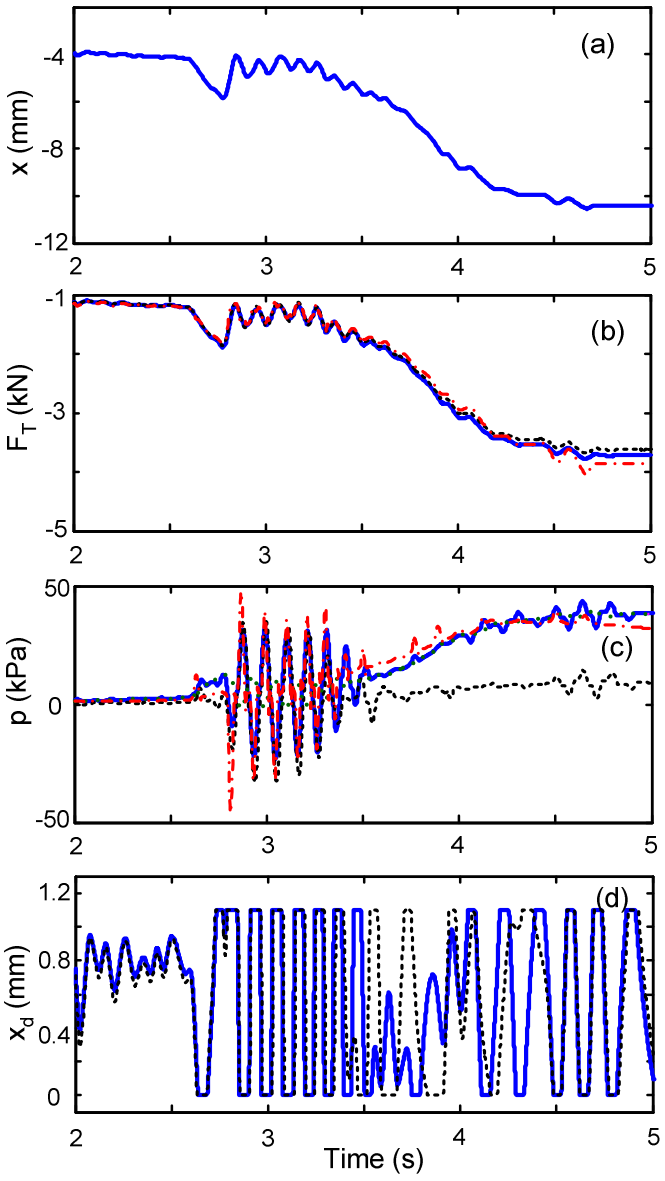


Fig. 12 Responses to a realistic profile excitation for a free decoupler mount D: (a) displacement excitation $x(t)$; (b) transmitted force $F_T(t)$; (c) chamber pressures; and (d) decoupler displacement $x_d(t)$. Key: -·-·-, measurement; -----, non-linear model prediction with a constant $C_{20}$; ——, non-linear $C_2(x_m)$ model prediction with $C_{2e} = C_{20}/5$; ·····, non-linear $C_2(x_m)$ model prediction for $p_2(t)$ with $C_{2e} = C_{20}/5$.

## ACKNOWLEDGMENTS

We acknowledge the experimental efforts of M. Tiwari and J. Sorenson from 1999 to 2002 (on mount D). Those studies were financially supported by the Ford Motor Company. Dr. J. H. Lee is thanked for his comments and suggestions.

## REFERENCES

1. R. Singh, G. Kim and P. V. Ravindra, "Linear analysis of automotive hydro-mechanical mount with emphasis on decoupler characteristics", J. Sound Vib. 158, 219-243 (1992).
2. G. Kim and R. Singh, "Study of Passive and Adaptive Hydraulic Engine Mount Systems with Emphasis on Nonlinear Characteristics", J. Sound Vib. 179, 427-453 (1995).
3. J. E. Colgate, C. T. Chang, Y. C. Chiou, W. K. Liu and L. M. Keer, "Modeling of a Hydraulic Engine Mount Focusing on Response to Sinusoidal and Composite Excitations", J. Sound Vib., 184(3), 503-528 (1995).
4. T. J. Royston and R. Singh, "Study of Non-Linear Hydraulic Engine Mounts Focusing on Decoupler Modeling and Design", SAE Transactions – J. Passenger Cars, 106(2), 2759-2769, (1997).
5. T. Jeong and R. Singh, "Inclusion of Measured Frequency-and Amplitude-Dependent Mount Properties in Vehicle or Machinery Models", J. Sound Vib. 245, 385-415 (2001).
6. A. Geisberger, A. Khajepour and F. Golnaraghi, "Non-Linear Modeling of Hydraulic Mounts: Theory and Experiment", J. Sound Vib, 249(2), 371-397 (2002).
7. G. N. Jazar and M. F. Golnaraghi, "Non-Linear Modeling, Experimental Verification, and Theoretical Analysis of a Hydraulic Engine Mount", J. Vib. Control, 8(1), 87-116, (2002).
8. M. S. Foumani, A. Khajepour and M. Durali, "Application of Sensitivity Analysis to the Development of High Performance Adaptive Hydraulic Engine Mounts", J. Vehicle Sys. Dynamics, 39(4), 257-278 (2003).
9. M. Tiwari, H. Adiguna and R. Singh, "Experimental Characterization of a Nonlinear Hydraulic Engine Mount", Noise Control Eng. J. 51(1), 36-49 (2003).
10. H. Adiguna, M. Tiwari and R. Singh, "Transient Response of a Hydraulic Engine Mount", J. Sound Vib. 268, 217-248 (2003).
11. S. He and R. Singh, "Estimation of Amplitude and Frequency Dependent Parameters of Hydraulic Engine Mount Given Limited Dynamic Stiffness Measurements", Noise Control Eng. J., 53(6), 271-285 (2005).
12. Y. Yu, N. G. Naganathan and R. V. Dukkipati, "A Literature Review of Automotive Vehicle Engine Mounting Systems", J. Dynamic Sys, Measurement, and Control, 123(2), 186-194 (2001).
13. J. H. Lee, M. S. Bae and K. J. Kim, "Limitations of Mechanical Model With Lumped Mass in Representing Dynamic Characteristics of Hydraulic Mount", SAE Paper 2003-01-1466 (2003).
14. N. Tsujiuchi, T. Koizumi and K. Yamazaki, "Vibration Analysis of Engine Supported by Hydraulic Mounts", SAE Paper 2003-01-1465 (2003).
15. J. Christopherson and G. Nakhaie Jazar, "Dynamic Behavior Comparison of Passive Hydraulic Engine Mounts. Part 1: Mathematical Analysis", J. Sound Vib. 290, 1040-1070 (2006).
16. S. He and R. Singh, "Discontinuous Non-Linearities in the Hydraulic Engine Mount", revised manuscript submitted to J. Sound Vib. (2006).

## CONTACT

Professor Rajendra Singh
Acoustics and Dynamics Laboratory
Center for Automotive Research and
NSF I/UCRC Smart Vehicle Concepts Center
The Ohio State University
Email: singh.3@osu.edu
Phone: 614-292-9044
Website: www.AutoNVH.org